Supplementary Information

Impact of solvent-induced morphological changes on hole transfer dynamic during charge separation process

Dongchan Lee[a†], Chang-Mok Oh[b†], Jiho Ryu[a], Sung-Yeon Jang[c], In-Wook Hwang[b*] and Shinuk Cho[a*]

[a]Department of Physics and Energy Harvest Storage Research Center, University of Ulsan, Ulsan 44610, Republic of Korea.
[b]Advanced Photonics Research Institute, Gwangju Institute of Science and Technology, Gwangju 61005, Republic of Korea
[c]Department of Energy Engineering, School of Energy and Chemical Engineering, Ulsan National Institute of Science and Technology (UNIST), Ulsan 44919, Republic of Korea

[*]Corresponding Authors: (E-mail) sucho@ulsan.ac.kr (S.Cho), hwangiw@gist.ac.kr (I. Hwang)
[†]D. Lee and C. Oh contributed equally to this work.

Device Fabrication

All organic solar cell devices are fabricated with a conventional structure of indium tin oxide (ITO)/poly(3,4-ethylenedioxythiophene):poly(styrenesulfonate) (PEDOT:PSS)/active layer/Phen-NaDPO/Al. Patterned ITO glass was cleaned using an ultrasonication bath with detergent, acetone, and isopropyl alcohol for 10 min each. Cleaned ITO glass was dried for 60 min in a heated oven (110 ^{o}C) at ambient air and then UV-ozone treated for 30 min. The PEDOT:PSS solution (Clevios, AI4083) was spin-coated on ITO glass at 5000 rpm for 30 s and thermally annealed at 150^{o}C for 10 min. The active layer solutions were mixed with donor and acceptor materials with optimized conditions to fix the active layer thickness of 120 nm, (donor:acceptor = 1:1.2 w/w%, 16 mg/mL in chloroform (CF) and 19.8 mg/mL in chlorobenzene (CB) with 0.5 v/v% of chloronaphtalene additive). The active layer solutions were spin-coated at 5000 rpm (CF) and 1700 rpm (CB) for 30 s on the PEDOT:PSS layer. Phen-NaDPO was used cathode buffer layer dissolved in isopropyl alcohol with concentration of 0.5 mg/mL and the solution was spin-coated on active layer at 5000 rpm for 30 s. Finally, the metal electrode (Al, 100 nm) was deposited by thermal evaporation method under a high vacuum (<3x10^{-6} Torr).

Device characterization

The power conversion efficiencies of the devices were measured by current density-voltage (J-V) curves using a Keithley 2041 source meter unit under AM 1.5G solar simulator (100 mW/cm^2). The intensity of simulated sunlight was calibrated using a standard Si solar cell with a KG-3 filter (Newport Co.). External quantum efficiency (EQE) spectra of solar cells were measured using IQE-200B (Newport Co.). The absorption spectra of each active layer were measured using a UV-Vis spectrophotometer (Cary-5000, Agilent).

Morphology & Crystallinity properties

The surface morphologies of active layers were measured using atomic force microscope (AFM, Nanocute, SII Nano Technology Inc.). GIWAXS was measured at the Pohang Accelerator Laboratory on the PLSII- 9A U-SAXS beamline; the beam of wavelength 0.1103 nm was incident on the samples at the angle of 0.13°. GIWAXS patterns were estimated with a charge-coupled device (CCD) detector (Rayonix SX165, PI-SCX: 4300).

FTPS-EQE and EL measurements

Fourier-transform photocurrent spectroscopy (FTPS) was measured in a home-built FTPS setup, which consisted of a Fourier-transform infrared (FTIR) spectrometer (INVEIO-R, Bruker) equipped with a tungsten-halogen lamp and quartz beam splitter. The photocurrent produced by the solar cell under illumination was amplified using a low-noise preamplifier (SR570, Standford Research Systems) and fed back into the external detector port of the FTIR spectrometer. FTPS-EQE was calculated from a spectrum of a light source and FTPS signal. Electroluminescence (EL) signals passed through the integral sphere and were recorded using a highly sensitive spectrophotometer (MAYA 2000 Pro, Ocean Optics). The integral sphere and spectrophotometer were calibrated using a standard halogen calibration light source (HL-3-plus-INT-CAL, Ocean Optics). EQE_{EL} was calculated with the injected current versus EL spectrum unit of absolute irradiance.

Space-charge-limited current (SCLC) mobility measurement

The hole and electron mobilities of devices were measured by the SCLC model using device structures of ITO/PEDOT:PSS/active layers/MoO3/Ag (hole-only device) and ITO/ZnO/active layers/Phen-NaDPO/Al (electron-only device) with same active layer thickness of 120 nm. *J-V* curves of hole- and electron-only devices were measured and fitted by Mott-Gurney's law, as followed[1]:

$$J = \frac{9}{8}\mu\varepsilon_0\varepsilon_r\frac{V^2}{L^3} \quad (1)$$

where J is current density, μ is carrier mobility, ε_0 is the permittivity of free space (8.85 x 10^{-14} F/cm), ε_r is the relative dielectric constant of active layer, V is effective voltage, and L is the thickness of the active layer. Carrier mobility was derived from the slope at the SCLC region from $J^{1/2}$ versus V plots.

In addition, the hole and electron trap density of devices were calculated from SCLC mobility curves using the following equation[2]:

$$V_{TFL} = \frac{qn_tL^2}{2\varepsilon_0\varepsilon_r} \quad (2)$$

where V_{TFL} is the trap-filled limited voltage obtained from cross-point of ohmic region and trap-filled-limit SCLC region, q is the electric charge, L is the thickness of photoactive layer, ε_0 is the vacuum permittivity, ε_r is the relative dielectic constant, and n_t is the trap density.

Transient absorption (TA) and time-correlated single photon counting (TCSPC) measurements

Femtosecond TA spectra and decays were recorded using a home-made TA spectrometer combined with a femtosecond Ti:sapphire regenerative amplifier system (Hurricane, Spectra Physics) and multichannel spectrometer (NIR Quest, Ocean Insight). A pump pulse at 650 nm with a power density of ~1 μJ/cm^2 was produced using an optical parametric amplifier (IR-OPA, Spectra Physics) and a neutral density filter, while a broadband white-light continuum probe pulse was generated by focusing the 800 nm amplifier output into a sapphire window. TA signals in respective optical delays of pump and probe pulses were collected using an optical fiber coupled with multichannel spectrometers from Ocean Insight (NIR Quest). More details on this system were noted in the previous publication[3, 4]. The steady-state fluorescence spectra were measured using a Home-made fluorescence spectrophotometer (QE-Pro, Ocean Insight). The time-resolved fluorescence-decay profiles were recorded using a TCSPC system comprised of a picosecond laser (LDH-P-C-470, PicoQuant), a monochromator (SP-2150, Princeton Instruments), a multichannel plate photomultiplier tube (R3809U-51, Hamamatsu), and a photon counting module (**SPC-130-EM**, Becker & Hickl GmbH). The PL decay time constants were obtained by deconvolution fitting to a summation of exponential terms, i.e., $I(t) = A_1\exp(-t/\tau_1) + A_2\exp(-t/\tau_2)$, where $I(t)$ is the time-dependent PL intensity, A is the normalized amplitude, and τ is the fitted PL lifetime. The average decay times were obtained using $(A_1\tau_1 + A_2\tau_2)/(A_1 + A_2)$.

Marcus Theory

According to the Frank-Condon principle, the absorption and emission have to be symmetric exactly from the lowest vibronic state (intersection point) because the electronic transitions are faster compared with nuclear motions. Similarly, charge transfer state (E_{CT}) can be determined by the Marcus theory, which explains the rates of electron transfer reactions, and the spectral region of CT absorption and emission are expressed[5]:

$$\mathrm{EQE(E)} \cdot E = \frac{\alpha_{absorption}}{\sqrt{4\pi\lambda k_B T}} exp\left[-\frac{\left(E_{CT} + \lambda - E\right)^2}{4\lambda k_B T} \right] \quad (3)$$

$$I_f / E = \frac{\alpha_{emission}}{\sqrt{4\pi\lambda k_B T}} exp\left[-\frac{\left(E_{CT} - \lambda - E\right)^2}{4\lambda k_B T} \right] \quad (4)$$

where α is coupling constant, λ is reorganization energy, k_B is Boltzmann's constant, T is temperature, I_f is the emission rate, and E is the corresponding energy to absorption/emission spectrum.

Energy loss model

The energy loss based on the detailed balance and reciprocity can be expressed sum of three components as follows[6]:

$E_{loss} = \Delta E_1 + \Delta E_2 + \Delta E_3$

$$= \left(E_g - qV_{oc}^{SQ}\right) + \left(qV_{oc}^{SQ} - qV_{oc}^{rad}\right) + \left(qV_{oc}^{rad} - qV_{oc}\right) \quad (5)$$

where E_{oc}^{rad} is radiative limited V_{oc} in consider of EQE and V_{oc} is open-circuit voltage measured from the current density-voltage (*J-V*) curve. ΔV_1 is voltage loss due to mismatches angle between incident sunlight and emission and carrier concentration between generation and the radiation from the cell. ΔV_2 is the radiative voltage loss by the imperfection of EQE since the V_{oc}^{SQ} considers the assumption of 100% of EQE, and ΔV_3 is non-radiative voltage loss due to the non-radiative recombination.

Referring to reciprocity theorem, qV_{oc}^{rad} states the radiative limit in which including the EQE of solar cell[7]:

$$V_{oc}^{rad} = \frac{k_B T}{q} ln\left[\frac{J_{sc}}{J_{0,rad}} + 1\right] = \frac{k_B T}{q} ln\left[\frac{q\int_0^\infty \Omega_{PV}(E)\phi_{sun}(E)dE}{q\int_0^\infty \Omega_{PV}(E)\phi_{BB}(E)dE} + 1\right]. \quad (6)$$

where

$$\phi_{BB}(E) = \frac{2\pi E^2}{h^3 c^2} \exp\left[-\frac{E}{k_B T} \right] \quad (7)$$

is blackbody radiation from the semiconductor and $\Omega_{PV}(E)$ is EQE of solar cell. Herein, V_{oc}^{rad} must be the V_{oc} of the solar cell in situation that radiative recombination in the only process in the total recombination. Thus, the

non-radiative energy loss is defined as the difference of V_{oc}^{rad} and real V_{oc} as described in **Eq.5**. By the definition of total energy loss, ΔE_3 is the residual value of voltage losses above, i.e.,

$$\Delta E_3 = E_{loss} - (\Delta E_1 + \Delta E_2) = qV_{oc}^{rad} - qV_{oc}. \quad (8)$$

Meanwhile, EQE_{EL} is defined as the radiative recombination current divided by the injected current for EL emission:

$$EQE_{EL} = \frac{J_{emitted}(V)}{J_{inject}(V)} = \frac{J_{rad}(V)}{J_{rad}(V) + J_{non-rad}(V)} . (9)$$

Because the EQE_{EL} refers how the radiative recombination possesses in total recombination ΔV_3 is proportional to -ln(EQE_{EL}):

$$\Delta V_3 = V_{oc}^{rad} - V_{oc} \cong -\frac{k_B T}{q} ln[EQE_{EL}] . (10)$$

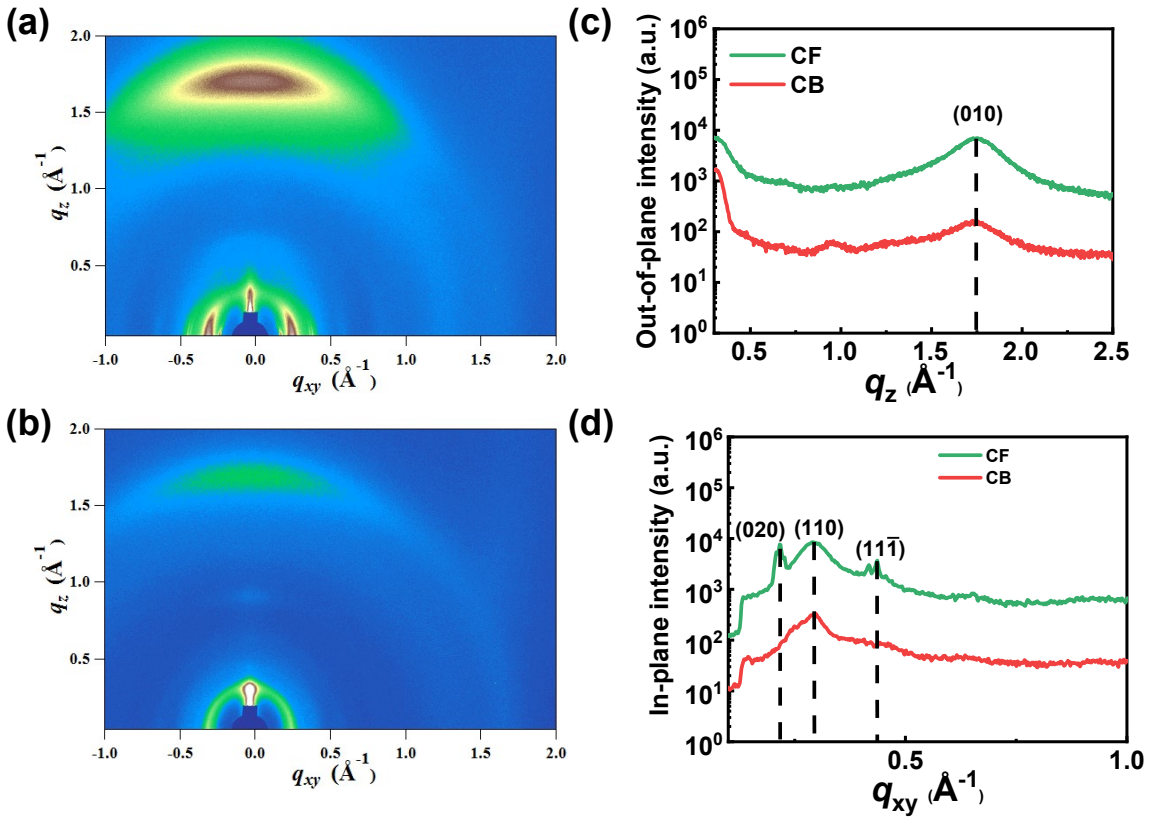

Fig. S1. GIWAXS pattern of (a) PM6:Y6-CF and (b) PM6:Y6-CB films. GIWAXS patterns were 2D-line profiled along (c) out-of-plane and (d) in-plane directions.

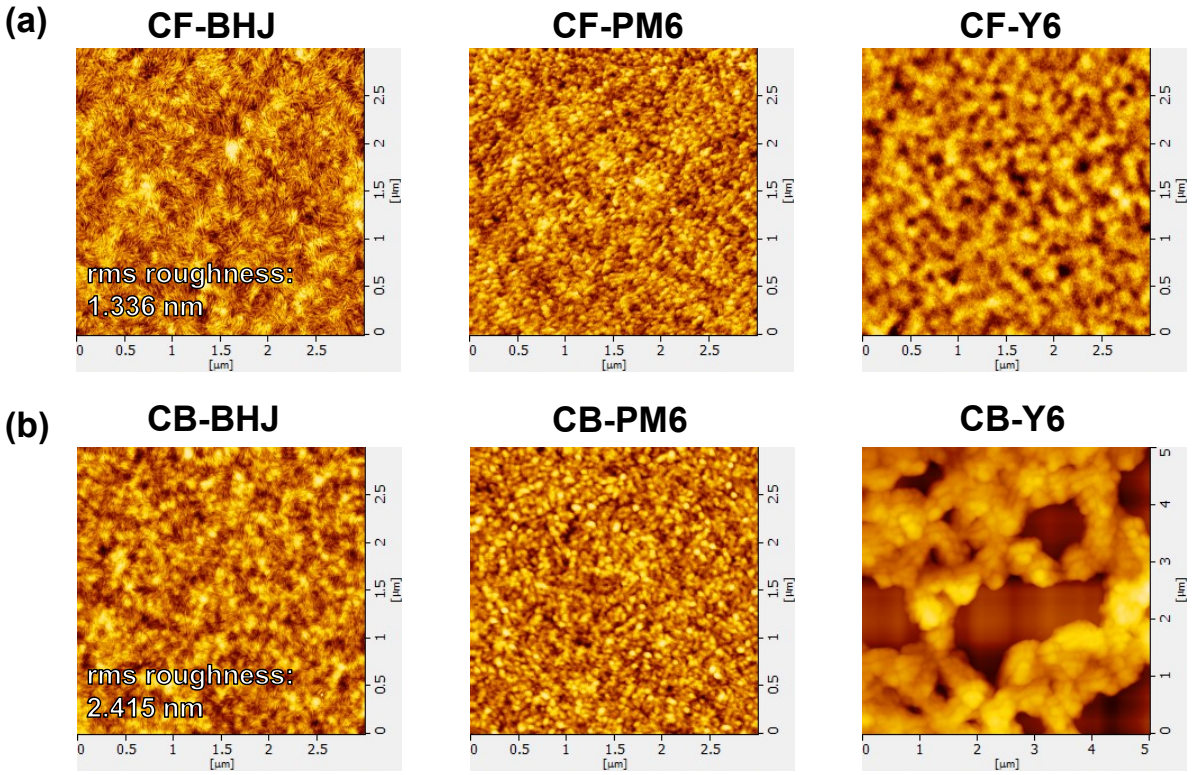

Fig. S2. AFM topographic images of (a) CF- and (b) CB- BHJ, PM6, and Y6 films.

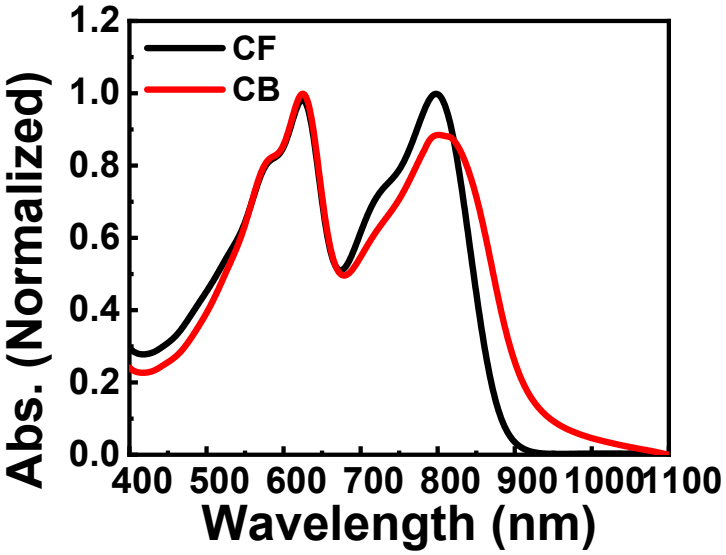

Fig. S3. Absorption spectra of PM6:Y6-CF and PM6:Y6-CB films.

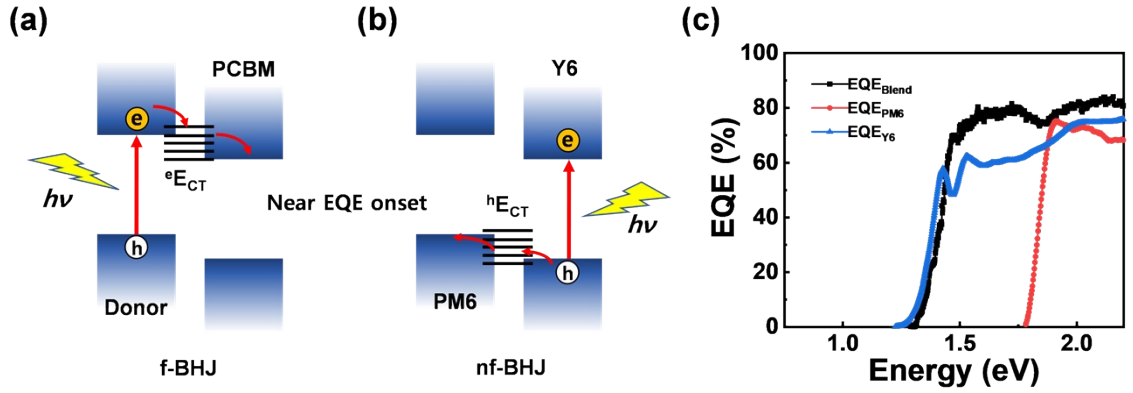

Fig. S4. Schematic diagram of charge transferring mechanism in (a) f-BHJ and (b) nf-BHJ organic solar cells. (c) EQE spectra of PM6:Y6 blend, PM6, and Y6 only device.

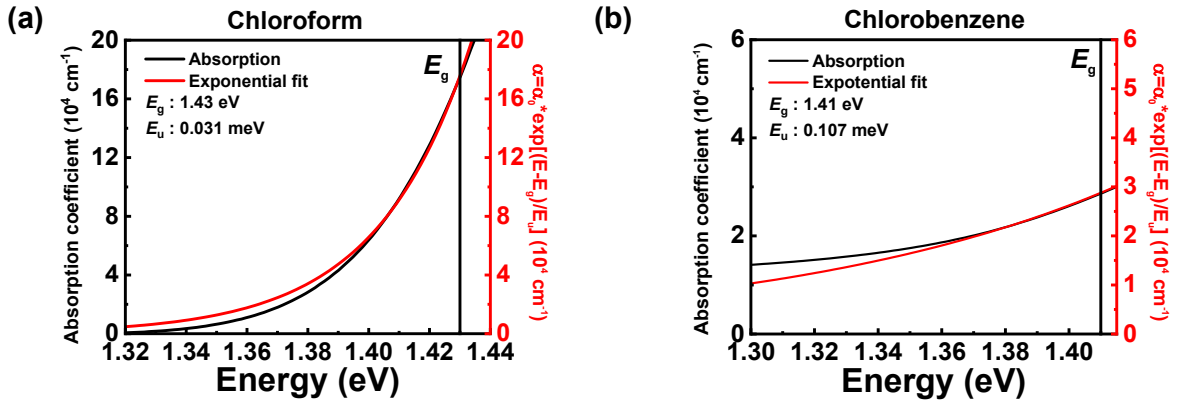

Fig. S5. Urbach energy calculation by exponential fit at absorption onset for (a) CF- and (b) CB- processed film. Note that E_g is an optical band gap which is distinguished from the listed in **Fig. S7** and **Table S1**.

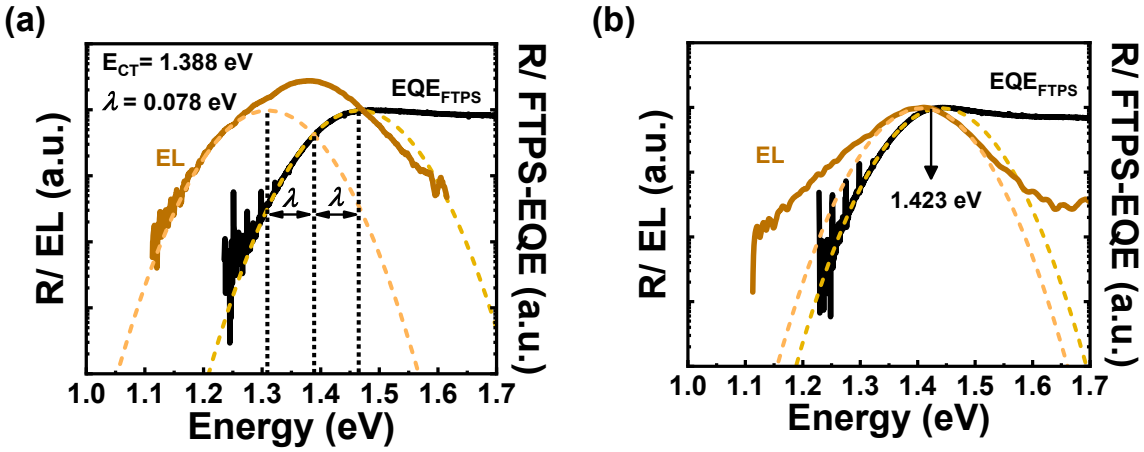

Fig. S6. E_{CT} determination of (a) PM6:Y6-CF and (b) PM6:Y6-CB devices based on Marcus theory (see Marcus Theory part in supporting information). The exact E_{CT} value could not be determined in PM6:Y6-CB device since the higher effective ${}^{h}E_{CT}$ absents. Consequently, overlapped region of FTPS-EQE and EL is larger than PM6:Y6-CF, which is singlet transition region of acceptor.

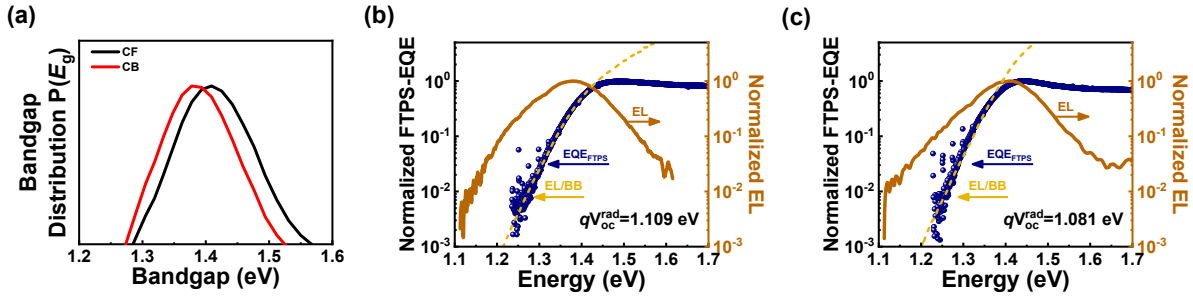

Fig. S7. (a) Bandgap distribution of CF- and CB-processed devices based on the detailed balance and reciprocity theorem[6]. (b) Energy loss analysis of CF- and (c) CB-processed device. EL/BB was fit to onset of FTPS-EQE to determine qV_{oc}^{rad}.

Table S1. Energy loss results of PM6:Y6-CF and PM6:Y6-CB devices.

Solvent	E_g	qV_{OC}^{SQ}	qV_{OC}^{rad}	$\boldsymbol{qV}_{\mathbf{oc}}$	ΔE_1	ΔE_2	ΔE_3	$\boldsymbol{E}_{\mathbf{loss}}$
CF	1.408	1.151	1.109	0.873	0.257	0.042	0.236	0.535
CB	1.386	1.130	1.081	0.817	0.256	0.049	0.286	0.569

* Unit : eV

References

[1] N. F. Mott and R. W. Gurney, Electronic Processes in Ionic Crystals 1st ed., Oxford University Press, Oxford, 1940.

[2] M. A. Lampert, *Phys. Rev.*, 1956, **103**, 1648.

[3] C.-M. Oh, J. Lee, S. H. Park and I.-W. Hwang, *Spectrochim. Acta A Mol. Biomol. Spectrosc.*, 2021, **250**, 119227.

[4] C.-M. Oh, J. Lee, S. H. Park and I.-W. Hwang, *J. Phys. Chem. Lett.*, 2021, **12**, 6418–6424.

[5] R. A. Marcus, *J. Phys. Chem.*, 1989, **93**, 3078-3086.

[6] T. Kirchartz and U. Rau, *Phys. Status Solidi A*, 2008, **205**, 2737–2751.

[7] U. Rau, B. Blank, T. C. M. Müller and T. Kirchartz, *Phys. Rev. Applied*, 2017, **7**, 044016.